ACS APPLIED MATERIALS & INTERFACES

Research Article

www.acsami.org

Device Stability and Light-Soaking Characteristics of High-Efficiency Benzodithiophene–Thienothiophene Copolymer-Based Inverted Organic Solar Cells with F-TiO_x Electron-Transport Layer

Fang Jeng Lim,[†,‡] Ananthanarayanan Krishnamoorthy,[‡] and Ghim Wei Ho*[,†]

[†]Department of Electrical and Computer Engineering, National University of Singapore, Block EA No. 06-10, 9 Engineering Drive 1, 117575 Singapore

[‡]Solar Energy Research Institute of Singapore, National University of Singapore, 7 Engineering Drive 1, 117574 Singapore

Supporting Information

ABSTRACT: Organic solar cells (OSC) based on low-band-gap thienothiophene–benzodithiophene copolymer have achieved relatively high efficiency (7–9%) in recent times. Among this class of material, poly({4,8-bis[(2-ethylhexyl)oxy]benzo[1,2-b:4,5-b′]dithiophene-2,6-diyl}{3-fluoro-2-[(2-ethylhexyl)carbonyl]-thieno[3,4-*b*]thiophenediyl}) (PTB-7) is one of the high-efficiency materials reported for OSC. However, this material seems to be intrinsically unstable compared to the commonly used workhorse polymer, poly(3-hexylthiophene) (P3HT), especially when illuminated in air. Inverted device architecture is usually adopted to improve device stability, but the device stability using PTB-7 is not yet well-understood. In this work, a systematic degradation study on a PTB-7:$PC_{71}BM$-based inverted OSC employing F-TiO_x as electron-transport layer (ETL) was conducted for the first time. Air stability, photostability in inert atmosphere, and photostability under ambient conditions of the device were separately carried out to understand better the polymer behavior in inverted OSC. The device's air stability with different polymer absorber layers was studied by exposing the devices in air for up to 1500 h. Because of the long and easily cleavable alkoxy side chains in the polymer backbone, a PTB-7:$PC_{71}BM$-based inverted OSC device is highly susceptible to oxygen and moisture when compared to a P3HT:$PC_{61}BM$-based device. In addition, with the presence of F-TiO_x ETL, a significant reduction in light-soaking time was also observed in PTB-7:$PC_{71}BM$ inverted OSC for the first time. The TiO_x/organic interface was found to be responsible for the reduction in the light-soaking time.

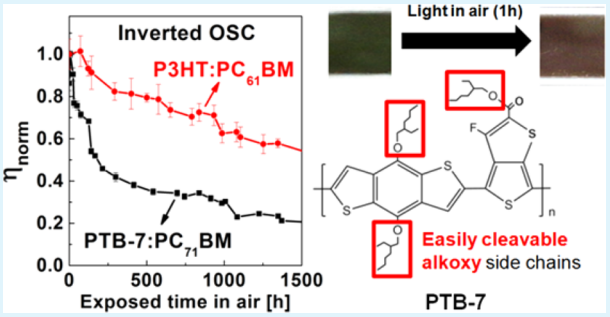

KEYWORDS: *degradation, light soaking, benzodithiophene, low band-gap polymers, fluorinated titanium dioxide, inverted organic solar cell*

INTRODUCTION

Solution-processed organic solar cells (OSC) have made significant progress in recent times with device efficiency reaching 10%.[1−3] However, the device stability of OSCs still needs serious improvement if they are to be used in outdoor applications. One way of improving device stability is by employing inverted architecture. In this architecture, the positions of the hole-transport layer (HTL) and electron-transport layer (ETL) are interchanged, resulting in the charges being collected in the opposite direction across the device compared to its noninverted or conventional counterpart. Inverted organic solar cells (IOSC) provide better stability compared to noninverted devices via the following key modifications: (1) shifting the hygroscopic PEDOT:PSS away from the ITO surface to prevent unintended etching and (2) replacing the low-work-function metal contact (Al) with a high-work-function metal (Ag) to prevent oxidation.[4,5] Impressive studies have been carried out on P3HT:$PC_{61}BM$-based devices to understand its degradation behavior under standard operating conditions.[6−9] To further increase the device efficiency of OSCs over 10%, development of new photoactive material based on low-band-gap polymers have been carried out.[10,11] Low-band-gap polymers have been used to increase device efficiency by extending the absorption of the photoactive material into the longer wavelength region, and this has been achieved by adopting the strategy of employing alternating electron-rich (donor) moieties and electron-poor (acceptor) moieties to establish a push–pull interaction that results in the band-gap tailoring.[12−18] Because of its symmetric and planar π-conjugated structure, benzodithiophene (BDT) has proven to be one of the most efficient donor materials for high-performance photovoltaic devices with PCBM acceptors. This property is also expected to provide tight and regular stacking for the BDT-based conjugated polymers, which in turn could

Received: March 18, 2015
Accepted: May 11, 2015
Published: May 11, 2015

DOI: 10.1021/acsami.5b02383
ACS Appl. Mater. Interfaces 2015, 7, 12119−12127

enhance the electron delocalization and interchain interaction.[19−21]

Among these polymers, poly({4,8-bis[(2-ethylhexyl)oxy]-benzo[1,2-b:4,5-b′]dithiophene-2,6-diyl}{3-fluoro-2-[(2-ethylhexyl)carbonyl]thieno[3,4-*b*]thiophenediyl}) (PTB-7) shows a high efficiency of 7−9% in both conventional and inverted organic solar cells.[1,14,16,22] This polymer consists of alternating benzodithiophene (BDT) and thienothiophene (TT) moieties as its backbone. Despite being able to achieve high device efficiency, the low device lifetime of PTB-7 greatly hinders its applicability in organic solar cells, and the reason attributed to this is a side-chain oxidation caused by exposure to light in air.[23] The oxidation of the material consequently alters its absorption profile, leading to poor device stability. Razell-Hollis et al. conducted an in situ Raman spectroscopy study on PTB-7:$PC_{71}BM$ film with exposure to light in air for 10 min and concluded that the degradation takes place because of the oxidation of benzodithiophene functional groups, which alters the electron density of the neighboring thienothiophene unit and further triggers conjugation-breaking cycloaddition of O_2.[24] However, most of the device degradation studies until now were carried out in conventional device architecture, and little has been known about the degradation behavior of this material when employed in inverted architecture. Keeping this in mind, the present study is undertaken to further understand the degradation behavior of PTB-7:$PC_{71}BM$ blend under exposure to air, light, and the combination of both in the inverted architecture.

Though inverted organic solar cells (IOSC) exhibit significantly better device stability compared to standard-architecture OSC under ambient conditions, a reversible light-soaking treatment is required when an n-type oxide is used as a selective ETL in IOSC. Because this effect is reversible,[25−27] the device has to be activated repeatedly at each dark−light cycle (every morning if used in outdoor application) before it can function in full capacity. Hence, this effect should be addressed for improved device practicality. A typical device with TiO_x as ETL would require approximately 10 min under AM1.5 illumination to reach its maximum efficiency.[28,29] Light-soaking time of 15 min was needed when Al-doped ZnO (AZO) was used as the ETL.[30] Impurity-modified metal oxides have also been used by various groups to address the light-soaking issue.[29,31] Recently, we have reported for the first time on the use of fluorinated TiO_x as the ETL to overcome the light-soaking issue in P3HT:PCBM-based inverted organic solar cells.[29] We have concluded that the ITO/TiO_x interface is responsible for the reduction of light-soaking time because of the change in TiO_x work function that narrows the barrier width between the two interfaces.[29] However, the other interface, TiO_x/organic layer, may also play a role in the device light-soaking properties. It is thus important to investigate the contribution from this interface to the light-soaking time reduction.

In this work, we have conducted a systematic study on the air stability, photochemical stability, photo-oxidation stability, and light-soaking characteristics of PTB-7:$PC_{71}BM$-based inverted organic solar cells with fluorinated TiO_x (F-TiO_x) as the ETL.

RESULTS AND DISCUSSION

Device Performance. PTB-7:$PC_{71}BM$ and P3HT:$PC_{61}BM$ were used as the photoactive absorber layer in this study. For noninverted (conventional) organic solar cells, the device architecture was ITO/PEDOT:PSS (50 nm)/PTB-7:$PC_{71}BM$ (100 nm)/Ca (5 nm)/Al (100 nm). For inverted organic solar cells, F-TiO_x was used as the ETL because it was found to reduce the light-soaking time significantly.[29] The corresponding device architecture was ITO/F-TiO_x(80 nm)/PTB-7:$PC_{71}BM$ (100 nm) (or P3HT:$PC_{61}BM$ (200 nm))/PEDOT:PSS-CFS31 (50 nm)/Ag. The device fabrication steps are described in detail in the Experimental Section. The device architectures are depicted in Figure 1a. Scheme 1 shows the chemical structures

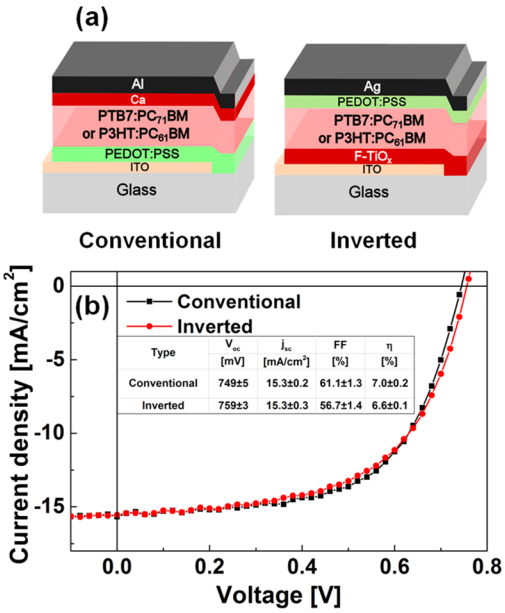

Figure 1. (a) Illustration of the device architecture for organic solar cells with conventional (left) and inverted (right) architecture. (b) Typical *j*−*V* characteristics of conventional and inverted organic solar cells and the corresponding device parameters (with average and standard deviation of the parameters over at least six devices included, inset table).

of the donor polymers P3HT and PTB-7 used in this work. All devices, unless otherwise stated, were subjected to degradation without encapsulation.

A series of OSC devices with both conventional and inverted architectures were fabricated for lifetime study in this work. Figure 1b shows the *j*−*V* characteristics of the fresh conventional and inverted PTB-7:$PC_{71}BM$-based OSC devices. (See Figure S1 in the Supporting Information for P3HT:$PC_{61}BM$-based OSC.) Both types of device exhibit

Scheme 1. Chemical Structures of Poly(3-hexylthiophene) (P3HT) and Polythieno-[3,4-*b*]-thiophene-co-benzodithiophene (PTB-7) Polymers Used in This Study

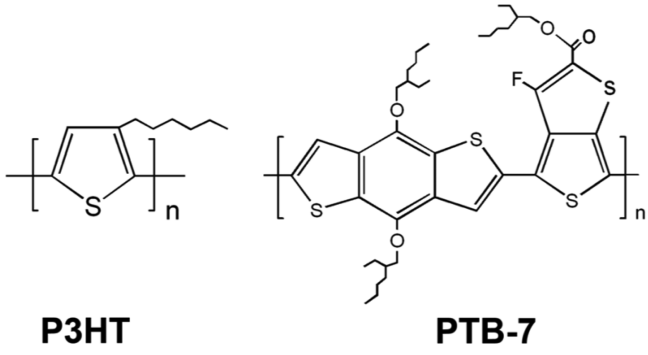

DOI: 10.1021/acsami.5b02383
ACS Appl. Mater. Interfaces 2015, 7, 12119−12127

similar efficiencies (~7%). This result suggests that the use of F-TiO_x does not significantly affect device performance when it is used as ETL in inverted OSC.

Air Stability. The air stability of as-prepared IOSC with F-TiO_x ETL was investigated by storing the device under dark and ambient conditions while monitoring its efficiency (η) over time, in accordance to the International Summit on Organic Photovoltaic Stability (ISOS) D-1 shelf scheme.[32] The device lifetime study of PTB-7:$PC_{71}BM$ in both device architectures is shown in Figure 2a. The samples were subjected to exposure

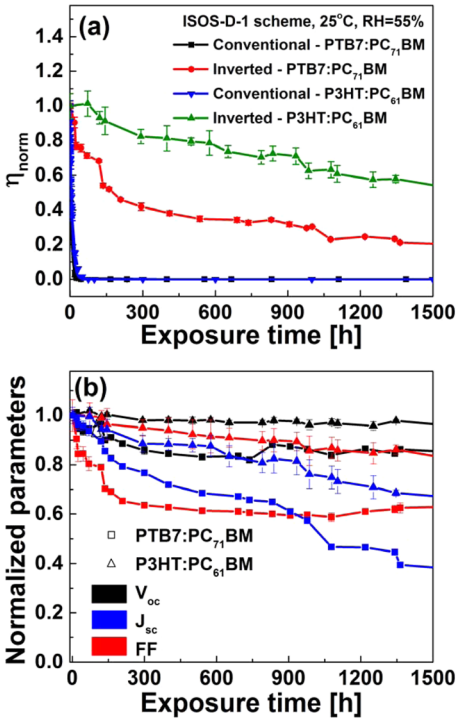

Figure 2. (a) Normalized efficiencies of the PTB-7:$PC_{71}BM$ conventional (black squares) and inverted (red circles) architectures under continuous exposure to air under dark, ambient condition (ISOS-D-1 shelf scheme) for 1500 h. P3HT:$PC_{61}BM$ conventional (blue triangles) and inverted devices (green triangles) are used as control devices to compare the stability of PTB-7-based device; (b) Normalized open-circuit voltage (black symbols), short-circuit current density (blue symbols) and fill factor (red symbols) for inverted PTB7:$PC_{71}BM$ (□) and P3HT:$PC_{61}BM$ (△). Normalized error bars correspond to the standard deviation for six devices, which were calculated on the basis of the initial value of the device parameters. Because the efficiencies of the devices differ, this accounts for the large difference in the error bars between P3HT:$PC_{61}BM$ and PTB7:$PC_{71}BM$.

under dark, open-circuit conditions at ambient atmosphere. The device performances were measured periodically over the course of 1500 h (63 days). As a control device, ITO/F-TiO_x/P3HT:$PC_{61}BM$/PEDOT:PSS/Ag was used to compare with the PTB-7-based device, and the data is also shown in the same figure. As expected, PTB-7:$PC_{71}BM$ IOSC is significantly more stable than its noninverted counterpart, retaining 70% of its initial device efficiency at ~120 h of air exposure, whereas the noninverted device degrades completely within the first 24 h of exposure. The observed degradation in the conventional device architecture is attributed to the following: (1) the attack of oxygen molecules from the easily oxidized Al metal contact into the photoactive layer, (2) etching of the ITO surface by acidic PEDOT:PSS, and (3) ingress of moisture into the photoactive materials.[5] All these processes would trigger the polymer to undergo oxidation and form oxygen-induced traps, which will result in the deterioration in the device performance.[9] However, inverted device architecture resolves most of the aforementioned issues: (1) Al was replaced by a more air-stable Ag as metal contact and (2) PEDOT:PSS is moved away from the ITO (preventing etching).

It is noteworthy that because of the direct exposure of PEDOT:PSS in air the moisture ingress from the hole-transport layer into the photoactive material is still possible in inverted structure. Furthermore, Norrman et al. have previously reported that the hygroscopic PEDOT:PSS in an inverted organic solar cell has a high water uptake when exposed to air in a dark environment, which corresponds to the ISOS-D-1 shelf scheme conducted in this study.[4] As a result, the device is highly sensitive to moisture-induced degradation. Interestingly, when compared to P3HT:$PC_{61}BM$ IOSC, the device lifetime of PTB-7:$PC_{71}BM$ IOSC is significantly shorter. P3HT:$PC_{61}BM$ IOSC could maintain 80% of its initial efficiency up to 600 h of exposure, whereas PTB-7:$PC_{71}BM$ IOSC already falls below 80% at the first 22 h. Because the attack of oxygen molecules from the easily oxidized Al metal contact into the photoactive layer and the etching of the ITO surface by acidic PEDOT:PSS have been circumvented in the inverted device,[4,5] the moisture ingress seems to be the remaining factor for the observed degradation. It has been reported previously that the hydroxylation of PTB-7 could change the polymer structure and render inferior charge transport property.[24]

In a closer look at the parameters in the inverted device (Figure 2b), the open-circuit voltage (V_{oc}), short-circuit current density (j_{sc}), and fill factor (FF) for the inverted devices decrease over exposure time in air. The decrease in V_{oc} would imply the presence of recombination losses, which may be caused by the change in work function of the hole-transport layer (PEDOT:PSS) because of the effect of moisture. Hence, the water absorbed by PEDOT:PSS will eventually diffuse through and react with the underlying photoactive layer. From Figure 2b, the moisture effect seems to influence PTB-7 in a greater scale compared to P3HT. This effect can be explained by the presence of long alkoxy substituents (2-ethylhexyl-oxy) in the BDT and TT groups in PTB-7, which is generally more susceptible to degradation compared to P3HT, where only a simple alkyl (hexyl) side chain is present (Scheme 1).[33] Furthermore, the nanomorphology of PTB-7 may also have been altered throughout the degradation period, as observed by a drastic decline in its j_{sc}.[34] As a result, the moisture attack accounts for the greater decrease in j_{sc} and FF in the PTB-7-based device compared to those in the P3HT-based device.

Photochemical Stability in N_2 Atmosphere. Despite the OSC devices being reasonably well-protected from oxygen and moisture through encapsulation, degradation would still occur over time. It is thus important to understand the behavior of the photoactive materials under illumination in the absence of oxygen and moisture. To rule out the effects of polymer oxidation, the photochemical stability of PTB-7:$PC_{71}BM$-based devices were studied by illuminating the samples under AM1.5G in a N_2-filled glovebox (oxygen and moisture < 1 ppm). The $j-V$ characteristics were acquired in situ during the illumination inside the glovebox. Indeed, the result shown in Figure 3 strongly suggests that the degradation of organic solar cells is not necessarily caused by oxygen and moisture alone. Direct absorption of UV−visible photons by the chromophores

DOI: 10.1021/acsami.5b02383
ACS Appl. Mater. Interfaces 2015, 7, 12119−12127

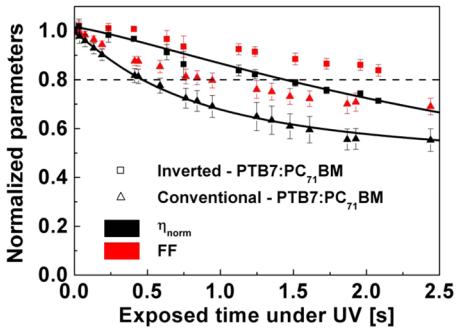

Figure 3. Normalized efficiency (black symbols) and fill factor (red symbols) of the PTB-7:$PC_{71}BM$ conventional (□) and inverted (△) architectures under continuous exposure to AM 1.5G in a nitrogen-filled glovebox (absence of oxygen). Dotted horizontal line indicates the lifetime (T_{80}) of each device. Black lines represent the fitted degradation profile according to experimental data. Error bars are the standard deviation obtained from at least six devices, which were calculated on the basis of the initial value of the device parameters. Reproducibility of the inverted device seems to be better than the conventional device, as seen in the difference in their error values.

of aromatic polymers in the absence of oxygen could trigger various reactions such as photoinduced side chain rearrangement (such as photo-Fries reaction), chain scissions, and cross-linking.[7,35] Because illumination was carried out in the absence of oxygen and moisture, the degradation would be purely in the form of photochemical processes.

Given the above condition, the polymer PTB-7 is significantly unstable under illumination compared to other photoactive materials such as polythiophenes,[8,36] MDMO-PPV,[37] and ZnPc,[38] which can withstand at least 500 h without undergoing significant degradation under the same condition. This result could originate from the chemical structure of PTB-7 backbone, i.e., benzodithiophene (BDT) and thienothiophene (TT) moieties. These two groups of monomers, though providing an excellent push−pull interaction for band-gap tailoring, are more susceptible to chemical changes because of the long alkoxy side chains (in the case of PTB-7). The presence of the alkoxy side chains in polymers is known to have negative impact to the polymer stability because the C−O bond is readily cleavable under irradiation in the absence of oxygen.[37,39] As a result, the high performance and solution processability of this material would serve as a trade-off against its stability. Interestingly, the device lifetime of inverted architecture is better than that of conventional architecture. The device T_{80} lifetime (where efficiency drops to 80% of its initial value) of the IOSC (90 min) is three times longer than that of the conventional OSC (30 min). The degradation of the device performance is solely caused by a decrease of fill factor during illumination (Figure 3, red symbols), whereas the V_{oc} and j_{sc} remain stable (Figure S2 in the Supporting Information). The inferior fill factor can be explained by a possible light-induced morphological degradation in the photoactive material, which causes a decline in carrier transport and carrier recombination.[40] Hence, the reason for higher stability is attributed to the presence of the UV-filtering F-TiO_x ETL (80 nm) with a band gap of 3.4 eV ($\lambda \approx 360$ nm) in the inverted OSC. (See Figure S3 in the Supporting Information.) The TiO_x layer is known to protect the device from UV light owing to its high-band-gap properties.[41] The presence of an Al:ZnO UV filter between the light source and the device was also shown to be effective in improving the stability of PTB-7:$PC_{71}BM$ under illumination.[42] Hence, we may conclude that F-TiO_x could act as a UV-protective layer for PTB-7:$PC_{71}BM$ inverted device and could prevent the occurrence of photo-induced chemical processes, contributing to a more stable device compared to the one with a conventional architecture.

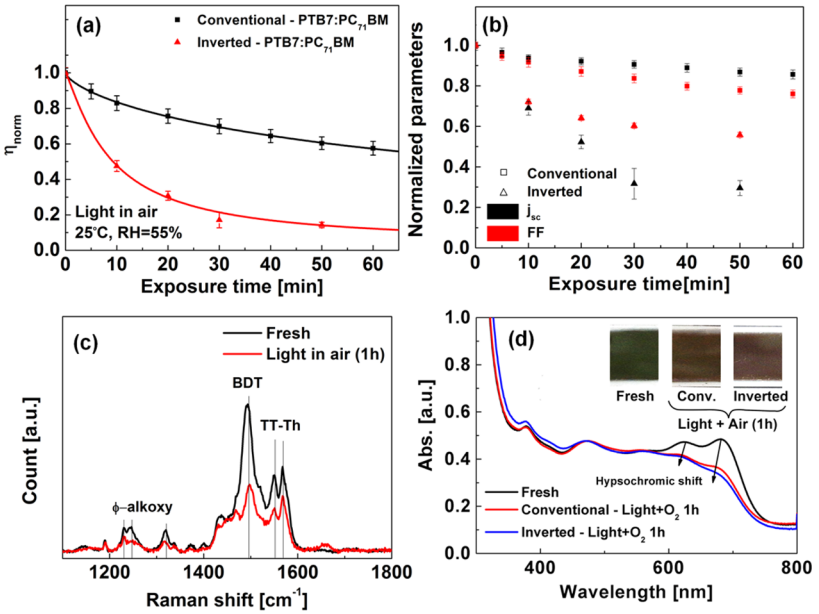

Figure 4. (a) Normalized efficiencies of the PTB-7:$PC_{71}BM$ conventional (black squares) and inverted (red triangles) architectures under continuous illumination in air. (b) Corresponding normalized j_{sc} (black symbols) and fill factor (red symbols) of conventional (squares) and inverted (triangles) architectures. Error bars are the standard deviation obtained from at least six devices, which were calculated on the basis of the initial value of the device parameters. (c) Raman spectra for fresh and degraded (illuminated in air for 1 h) neat PTB-7 films in air. (d) UV−vis absorption spectra of freshly prepared and degraded devices (light in air for 1 h) for both conventional and inverted architectures. Inset shows the film color changes before and after degradation.

DOI: 10.1021/acsami.5b02383
ACS Appl. Mater. Interfaces 2015, 7, 12119−12127

Comparing the photostability test with the air-stability test for the inverted device (Figure 2), T_{80} of the photoinduced degradation (1.5 h) is much shorter than the T_{80} of air- and moisture-induced degradation (22 h). The photoinduced degradation is therefore the more detrimental factor in the long term stability of PTB-7 in solar cell applications.

Photochemical Stability in Air. When freshly prepared PTB-7:$PC_{71}BM$ OSC and IOSC devices were exposed to light in air, significant deterioration in the performance was observed for both types of devices without encapsulation. The effect of oxygen and moisture under illumination accelerates the degradation dynamics in both types of PTB-7:$PC_{71}BM$ device. The photoactive material is especially vulnerable to oxygen and moisture under illumination. Various studies have also shown that oxygen is the dominating factor for polymer degradation, even in the case of inverted devices.[4,6,38] Indeed, the continuous illumination test shown in Figure 4a suggests that PTB-7:$PC_{71}BM$, regardless of the type of architecture, is vulnerable to oxygen- and moisture-induced degradation. The T_{80}/T_{50} times for conventional and inverted devices are 18/85 and 3/10 min, respectively. Further investigation of the device parameters in Figure 4b suggests a likelihood of chemical[42,43] and morphological[40,44,45] degradation in the photoactive layer because of the drastic decrease in j_{sc} and fill factor. The stable V_{oc} throughout the illumination (Figure S4 in the Supporting Information) suggests that there is no contribution of the transport layers to the device degradation. Thus, the photochemical degradation seems to occur only in the photoactive layer. Note that the device lifetimes are considerably shorter when compared to that of a P3HT:PCBM-based inverted device.[4] Norrman et al. has previously reported that when a P3HT:PCBM inverted device was exposed to light in a controlled environment, photo-oxidation of alkyl side chain will form R−COOH bonds within the first hour of illumination in air.[4] However, this is not the case for PTB-7 because the alkyl side chains in the polymer do not seem to participate in the photochemical degradation.[46] Raman spectra with fresh and degraded neat PTB-7 films were acquired (Figure 4d). The band between 1200 and 1350 cm^{-1} can be associated with phenylene−alkoxy (R−O) stretching in BDT.[37] The peaks at 1490, 1549, and 1570 cm^{-1} are associated with the C═C stretching mode of fused thiophene of BDT units, non-fluorinated thiophene, and fluorinated thiophene of TT units in PTB-7, respectively.[24] After 1 h of illumination in air, the Raman intensities of aforementioned peaks decrease. This phenomenon suggests possible cleavage in the alkoxy side chains in PTB-7 under illumination and subsequent breaks in the chain conjugation of the adjacent thiophene subgroups. Hence, the alkoxy side chains attached to the BDT and TT backbones are likely the reason for the accelerated photo-oxidation in PTB-7.

Interestingly, the conventional architecture has a better resistance toward oxygen than the inverted architecture within the testing period. There are two possible degradation pathways: (1) from PEDOT:PSS to photoactive layer and (2) from F-TiO_x to photoactive layer. First, PEDOT:PSS would undergo phase change under illumination in oxygen, and subsequent oxidation would occur in the PEDOT:PSS/organic interface.[4] Furthermore, direct exposure to light in air would render the photoactive layer and PEDOT:PSS to be oxidized to mainly form R−SO_x and R−COOH species.[4] For inverted devices, PEDOT:PSS is entirely exposed to air, as opposed to conventional devices, rendering it highly sensitive to water, thus accelerating the hydroxylation process under illumination. Second, despite the UV-filtering effect, the F-TiO_x layer in the inverted device may also provide a pathway for oxygen to attack the photoactive layer material. It has been reported that the oxygen may adsorb to and desorb from the metal oxide surface when illuminated in air.[29,47,48] During the illumination, the oxygen atoms could then readily attack, redistribute and oxidize the photoactive layer, causing a shorter device lifetime.

Because of the degradation pathways associated with inverted device and the inherent unstable nature of PTB-7, the device lifetime is worse compared to its conventional counterpart. As a result, there are various oxidation routes that could take place in PTB-7: (1) Singlet oxygen could be inserted into the C═C backbone, disrupting its conjugation arrangement.[23,42] or (2) The C−O bonds in the alkoxy side chain of PTB-7 would be highly susceptible to cleavage,[33] forming R−COOH and resulting in the break of π conjugation.[24] All these reactions would result in a reduction of conjugation length that leads to the bleaching of PTB-7 polymer. This phenomenon was clearly observed from the hypsochromic shift in the absorption peaks at 630 and 685 nm of PTB-7:$PC_{71}BM$ film (Figure 4d). It is well-known that the reaction of anthracene with oxygen will readily form a 9,10-endoperoxide derivative.[49] We believe that the BDT units also undergo the same reaction, producing the observed hypsochromic shift. This condition would disrupt the backbone conjugation of BDT units, thus causing an evident change in film color from dark blue to brown, corresponding to the change in the chromophore (Figure 4d, inset).

Light-Soaking Characteristics. The light-soaking properties of PTB-7:$PC_{71}BM$ inverted organic solar cells is vital to their practicality. It is important to realize the negative influence of the light-soaking property on the device from the perspective of outdoor applications. The reversible light-soaking effect signifies repeated photoactivation every morning in outdoor applications. A rough estimation of light-soaking time, based on 8 min under indoor AM1.5G illumination, would imply at least 1 h of outdoor light-soaking every morning (Figure S5 in the Supporting Information). In other words, for an average 8 h of daily sunlight, the first few hours of energy conversion every morning will be lost, despite its long device lifetime. Thus, it is important to address this issue by significantly reducing the required light-soaking time. Our previous reports have shown that F-TiO_x could significantly reduce the light-soaking time by more than 10-fold for an inverted P3HT:$PC_{61}BM$ device compared to conventional sol−gel TiO_x.[29] Hence, a P3HT:$PC_{61}BM$ device with sol−gel TiO_x and F-TiO_x ETL was used as a control device to compare with PTB-7:$PC_{71}BM$ device in this work, as shown in Figure 5. Light-soaking time (τ_{soak}) is defined as the time required for the efficiency to reach 95% of its maximum value ($\eta(\tau_{soak}) = 0.95\eta_{max}$); the light-soaking effect for various devices was tabulated in the figure inset. It is noteworthy that the light-soaking time, regardless of the photoactive material used, is also drastically reduced by employing F-TiO_x as the ETL. On one hand, we may conclude that the improvement in light-soaking properties of an IOSC is independent of the photoactive layer material. On the other hand, the use of F-TiO_x ETL is essential to improve the light-soaking issue. It was previously shown that the presence of fluorine in TiO_x matrix would decrease its work function and increase the overall carrier concentration; thus, it accelerates the UV-triggered trap-filling action.[29]

Apart from these effects from the ITO/F-TiO_x interface, the F-TiO_x/organic interface could also contribute significantly to

DOI: 10.1021/acsami.5b02383
ACS Appl. Mater. Interfaces 2015, 7, 12119−12127

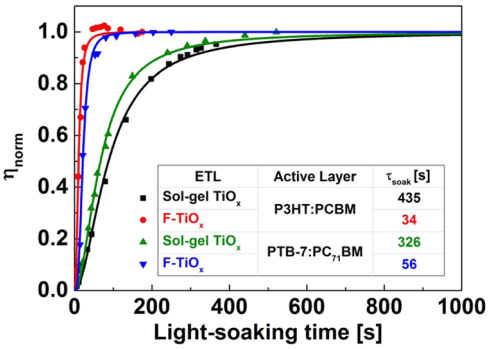

Figure 5. Light-soaking effect on the efficiency of fresh devices with sol−gel TiO_x or F-TiO_x layer for P3HT:$PC_{61}BM$ and PTB-7:$PC_{71}BM$ devices upon AM 1.5G illumination under N_2 atmosphere. Symbols represent experimental data, whereas the solid lines are fitted function (details at Table S1 in the Supporting Information). Embedded table shows the summary of the resulting light-soaking time (τ_{soak}) of each device.

the reduction in the light-soaking time. It was also found that the film morphologies of sol−gel TiO_x and F-TiO_x drastically differ. As clearly observed from the AFM images in Figure 6, sol−gel TiO_x has significantly smaller grain size compared to F-TiO_x because of the nature of coating techniques used. Titanium oxide coated with sol−gel technique hydrolyzes uniformly over the ITO substrates; whereas for F-TiO_x film, the film was formed by means of island and cluster growth.[29] As a result, the film is significantly rougher than sol−gel TiO_x, giving root-mean-square roughness (r_{rms}) values of 4.2 nm for F-TiO_x and 1.7 nm for sol−gel TiO_x. It is known that higher roughness of underlying metal oxide could increase the contact surface area with the subsequent layer for solar cell applications.[50,51] Ho et al. reported recently that ZnO nanorod ETL, which has a higher surface roughness, could effectively enhance the electron-transport properties by providing a larger contact area to transport electrons through the layer.[51] As a result, the higher roughness of the film is possibly another factor contributing to the significant reduction of light-soaking time. When there are more interactions between F-TiO_x and PTB-7:$PC_{71}BM$, electrons from the photoactive layer could contribute to the trap-filling of the metal oxide. It would result in a faster trap-filling action compared to that of sol−gel TiO_x in addition to the UV-excited electrons from the light-soaking treatment. Thus, the use of F-TiO_x ETL in PTB-7:$PC_{71}BM$ IOSC could produce a light-soaking-free device.

CONCLUSIONS

A systematic degradation study to investigate the air stability, photostability in inert atmosphere, and photostability in air of PTB-7:$PC_{71}BM$-based inverted organic solar cells with F-TiO_x as the ETL was conducted. The inverted device was proven to be stable when stored under dark and ambient conditions compared to a conventional device, largely because of the protection of photoactive layer by PEDOT:PSS and the high-work-function metal. However, because of the easily cleavable side chains in PTB-7 polymer, the PTB-7:$PC_{71}BM$ inverted device is significantly unstable compared to P3HT:$PC_{61}BM$ under the same conditions. Though the UV-filtering effect of F-TiO_x could contribute to the better photostability in N_2 atmosphere, the inverted device would still degrade over time by means of phototriggered chemical changes in the absence of oxygen. When the device is exposed to light in air, the inverted structure degrades significantly faster compared to the conventional device. The photo-oxidation effect from the direct exposure of PEDOT:PSS to air and the rearrangement of oxygen in F-TiO_x layer upon illumination in the inverted device may be the cause of the greater instability. Lastly, the light-soaking characteristics of ITO/F-TiO_x/PTB-7:$PC_{71}BM$/PEDOT:PSS/Ag were also studied and compared with those of the device using sol−gel TiO_x as the ETL. The significantly rougher F-TiO_x film could enable electrons to be transported from the photoactive layer to the F-TiO_x, thus contributing to the reduction of light-soaking at the F-TiO_x/organic interface.

EXPERIMENTAL SECTION

Materials. Chemical-bath-deposited F-TiO_x was prepared from ammonium hexafluorotitanate ($(NH_4)_2TiF_6$, 99.99%, Sigma-Aldrich) and boric acid (H_3BO_3, ≥ 99.99%, Sigma-Aldrich) as precursors. For sol gel-TiO_x, titanium isopropoxide (TTIP, 97%, Sigma-Aldrich), acetylacetone (AA, Sigma-Aldrich), and isopropanol (IPA, reagent-grade, Aik Moh Paints & Chemical Pte. Ltd.) were used. Polythieno-[3,4-*b*]-thiophene-*co*-benzodithiophene (PTB-7, 1-Material), phenyl-C_{71}-butyric acid methyl ester ($PC_{71}BM$, Nano-C), and poly(3,4-ethylenedioxythiophene): poly(styrenesulfonate) (PEDOT:PSS, Heraeus Clevios P VP AI 4083, product code M121, Ossila) were used as donor, acceptor, and hole-transport layers, respectively. Chlorobenzene (CB, Sigma-Aldrich) and 1,8-diiodooctane (DIO, Sigma-Aldrich) were used as the solvents for donor and acceptor. Capstone FS-31 (Dupont) was added into PEDOT:PSS prior to spin-coating. Silver (Ag) metal was purchased from K. J. Kurt Lesker & Co. (99.99%). Regioregular (>98%) poly(3-hexylthiophene) (P3HT, Sigma-Aldrich) and phenyl-C_{61}-butyric acid methyl ester ($PC_{61}BM$ − 99.5% purity, Nano-C) were used to fabricate the P3HT:PCBM inverted device to study the light-soaking effect. All the above-mentioned materials were used as received.

Solution Preparation. The precursor solutions for F-TiO_x films were prepared by mixing appropriate concentration of ammonium hexafluorotitanate ($(NH_4)_2TiF_6$, 99.99%, Aldrich) and boric acid (H_3BO_3). Both solutions were stirred separately for at least 10 min at room temperature before mixing. The stirred solutions were mixed and placed into a preheated bath at 40 °C before immersing ITO

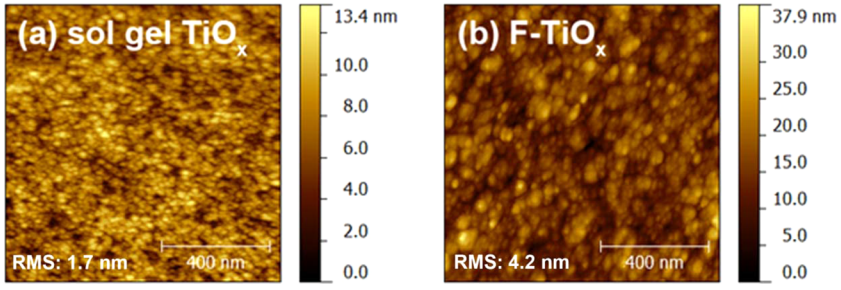

Figure 6. AFM topographic image for (a) sol−gel TiO_x and (b) F-TiO_x, indicating the corresponding root-mean-square roughness value.

DOI: 10.1021/acsami.5b02383
ACS Appl. Mater. Interfaces 2015, 7, 12119−12127

substrates into the bath for F-TiO_x deposition. The deposited film was finally annealed at 180 °C for 1 h. The precusor solution for sol−gel TiO_x was prepared by mixing titanium isopropoxide, acetylacetone, and isopropanol in volume ratio of 1:0.5:10. PTB-7:$PC_{71}BM$ blend was made in the ratio 1:1.5 (the concentration of PTB-7 was 12.5 mg/mL, whereas $PC_{71}BM$ was 18.75 mg/mL) in chlorobenzene (96%) and 1,8-diiodooctane (4%). P3HT:$PC_{61}BM$ blend was made in the ratio 1:0.8 (the concentration of P3HT was 15 mg/mL, whereas $PC_{61}BM$ was 12 mg/mL) in dichlorobenzene (DCB). The mixed solutions were stirred and heated at 60 °C overnight in a N_2 filled glovebox prior to spin-coating.

Device Fabrication. Both conventional (noninverted) and inverted bulk heterojunction organic solar cells based on PTB-7:$PC_{71}BM$ and P3HT:$PC_{61}BM$ were prepared on prepatterned tin doped indium oxide (ITO, Xinyan Technology Ltd.)-coated glass substrates. The sheet resistance of the ITO (thickness = 90 ± 10 nm) was found to be around 15−20 Ω/sq. The substrates were precleaned using a detergent solution, followed by successive ultrasonication in deionized water, isopropanol, and acetone for 15 min each. The substrates were then dried in an oven at 60 °C for 2 h. For the conventional device, this was followed by UV−ozone treatment for 15 min. Then, the PEDOT:PSS solution was filtered through a 0.45 μm cellulose filter and was later spin-coated at 5000 rpm for 60 s to obtain an approximately 50 nm thin layer on the ITO substrate, and the samples were then annealed in a N_2-filled glovebox at 140 °C for 20 min. A 100 nm layer of PTB-7:$PC_{71}BM$ was then spun onto the ETL at 1600 rpm for 20 s, and the resultant film was then annealed on a hot plate at 60 °C for 5 min. Ca (30 nm) and Al metal (100 nm) were then sequentially evaporated in 4×10^{-6} mbar through a predesigned shadow mask, resulting in an active device with an area of 9 mm^2. The completed device architecture is ITO/PEDOT:PSS/PTB-7:$PC_{71}BM$/Ca/Al. For the inverted device with F-TiO_x as the ETL, 80 nm of fluorinated TiO_x (F-TiO_x) was deposited onto ITO by immersing the ITO substrate into a chemical bath, comprised of 0.1 M ammonium hexafluorotitanate ($(NH_4)_2TiF_6$) and 0.2 M boric acid (H_3BO_3) at 40 °C for 90 min. Finally, the films were subjected to annealing at 180 °C for 1 h before transferring into a N_2-filled glovebox. For the inverted device with sol−gel TiO_x as the ETL, 80 nm of precursor solution was spun on ITO substrates and left to hydrolyze in air for 2 h before being annealed at 180 °C for 1 h. The annealed films were then transferred into a N_2-filled glovebox. A 100 nm layer of PTB-7:$PC_{71}BM$ was then spun onto the ETL at 1600 rpm for 20 s, and the resultant film was then annealed on a hot plate at 60 °C for 5 min. A 70 nm layer of PEDOT:PSS blended with CFS-31 (PEDOT:PSS-CFS-31) with volume ratio of 5.5% was then coated onto the active layer in air through a 0.45 μm cellulose filter and annealed at 140 °C for 1 min in the N_2-filled glovebox, as reported in our earlier work.[52] Ag metal (100 nm) was then thermally evaporated at 4×10^{-6} mbar through a predesigned shadow mask, resulting in an active device with an area of 9 mm^2. The completed device architecture is ITO/TiO_x/PTB-7:$PC_{71}BM$/PEDOT:CFS-31/Ag. For inverted devices with P3HT:$PC_{61}BM$, all fabrication steps are the same except for the photoactive layer spin-coating: P3HT:$PC_{61}BM$ was spun onto the ETL at 800 rpm for 30 s, and the resultant film was then annealed on a hot plate at 140 °C for 1 min. The completed device architecture is ITO/TiO_x/P3HT: $PC_{61}BM$/PEDOT:CFS-31/Ag.

Device Characterization. The current density−voltage ($j-V$) measurements were obtained under 1 sun illumination (ABET technologies Sun 2000 Solar Simulator) and a Keithley 2400 sourcemeter. The intensity was calibrated using a silicon reference cell (Fraunhofer ISE). The light-soaking treatment was done using the same lamp source, where the devices were continuously illuminated, and data were periodically acquired. The thicknesses of all layers were measured using a cross-sectional SEM image by using JEOL FEG JSM 6700F field emission SEM operating at 15 keV. All the fabrication steps, except coating of TiO_x and PEDOT:PSS, were performed inside a glovebox of N_2 atmosphere (Charslton Technologies, ≤ 1 ppm moisture and O_2). Cell degradation studies were carried out in various conditions: dark condition in air (25 °C, relative humidity 55%, ISOS-D-1 shelf scheme[32]), exposure to AM1.5G illumination in N_2-filled glovebox, and continuous illumination by solar simulator light source in ambient condition. Light-soaking experiments were conducted by monitoring the $j-V$ characteristics in situ while illuminating the freshly prepared device under AM1.5G. The UV−vis absorption spectra were acquired using Agilent Cary 7000 Universal Measurement Spectrophotometer in the wavelength range from 300 to 800 nm. Raman measurements were done using a Renishaw inVia microscope with a 50× objective in a backscattering configuration. The exciation source was a 514 nm (Ar ion) laser; spectra were obtained with a laser power of 0.25 mW and an acquisition time of 15 s. AFM images were collected using a Veeco Nano Scope IV Multi-Mode AFM system in tapping mode.

■ ASSOCIATED CONTENT

Supporting Information

$j-V$ characteristics for conventional and inverted P3HT:$PC_{61}BM$-based organic solar cells used as reference devices in the degradation study; normalized solar cell parameters (V_{oc}, j_{sc}, FF, efficiency) for conventional and inverted PTB7:PC71BM devices illuminated under inert atmosphere and in air; Tauc plot for estimation of band-gap energy of F-TiO_x; estimation of outdoor light-soaking time during a sunny day on the basis of indoor AM1.5G illumination data; fitting function for calculation of light-soaking time. The Supporting Information is available free of charge on the ACS Publications website at DOI: 10.1021/acsami.5b02383.

■ AUTHOR INFORMATION

Corresponding Author

*E-mail: elehgw@nus.edu.sg.

Notes

The authors declare no competing financial interest.

■ ACKNOWLEDGMENTS

SERIS is sponsored by the National University of Singapore (NUS) and Singapore's National Research Foundation (NRF) through the Singapore Economic Development Board (EDB). F.J.L. expresses his sincere gratitude to Singapore National Research Foundation (Energy Innovation Programme Office) for providing a Ph.D. scholarship. We gratefully acknowledge Dupont through MegaChem Limited, Singapore, for supplying Capstone FS-31.

■ REFERENCES

(1) He, Z.; Zhong, C.; Su, S.; Xu, M.; Wu, H.; Cao, Y. Enhanced Power-conversion Efficiency in Polymer Solar Cells Using an Inverted Device Structure. *Nat. Photonics* **2012**, *6*, 593−597.

(2) Woo, S.; Kim, W. H.; Kim, H.; Yi, Y.; Lyu, H. K.; Kim, Y. 8.9% Single-stack Inverted Polymer Solar Cells with Electron-rich Polymer Nanolayer-modified Inorganic Electron-collecting Buffer Layers. *Adv. Energy Mater.* **2014**, *4*, 1301692.

(3) Chen, J. D.; Cui, C.; Li, Y. Q.; Zhou, L.; Ou, Q. D.; Li, C.; Li, Y.; Tang, J. X. Single-junction Polymer Solar Cells Exceeding 10% Power Conversion Efficiency. *Adv. Mater.* **2015**, *27*, 1035−1041.

(4) Norrman, K.; Krebs, F. C. Degradation Patterns in Water and Oxygen of an Inverted Polymer Solar Cell. *J. Am. Chem. Soc.* **2010**, *132*, 16883−16892.

(5) Jørgensen, M.; Norrman, K.; Gevorgyan, S.; Tromholt, T.; Andreasen, B.; Krebs, F. Stability of Polymer Solar Cells. *Adv. Mater.* **2012**, *24*, 580−612.

(6) Madsen, M. V.; Norrman, K.; Krebs, F. C. Oxygen-and Water-induced Degradation of an Inverted Polymer Solar Cell: the Barrier Effect. *J. Photon. Energy* **2011**, *1*, 011104.

DOI: 10.1021/acsami.5b02383
ACS Appl. Mater. Interfaces 2015, 7, 12119−12127

(7) Rivaton, A.; Chambon, S.; Manceau, M.; Gardette, J. L.; Lemaître, N.; Guillerez, S. Light-induced Degradation of the Active Layer of Polymer-based Solar Cells. *Polym. Degrad. Stab.* **2010**, *95*, 278−284.
(8) Manceau, M.; Rivaton, A.; Gardette, J. L.; Guillerez, S.; Lemaître, N. Light-induced Degradation of the P3HT-based Solar Cells Active Layer. *Sol. Energy Mater. Sol. Cells* **2011**, *95*, 1315−1325.
(9) Set, Y. T.; Heinemann, M. D.; Birgersson, E.; Luther, J. On the Origin of the Quadrant I Semicircle in Intensity-modulated Photocurrent Spectra of P3HT:PCBM Bulk Heterojunction Solar Cells: Evidence of Degradation-related Trap-assisted Recombination. *J. Phys. Chem. C* **2013**, *117*, 7993−8000.
(10) Liao, S. H.; Jhuo, H. J.; Cheng, Y. S.; Chen, S. A. Fullerene Derivative-doped Zinc Oxide Nanofilm as the Cathode of Inverted Polymer Solar Cells with Low-bandgap Polymer PTB7-Th for High Performance. *Adv. Mater.* **2013**, *25*, 4766−4771.
(11) Intemann, J. J.; Yao, K.; Li, Y. X.; Yip, H. L.; Xu, Y. X.; Liang, P. W.; Chueh, C. C.; Ding, F. Z.; Yang, X.; Li, X.; Chen, Y.; Jen, A. K. Y. Highly Efficient Inverted Organic Solar Cells through Material and Interfacial Engineering of Indacenodithieno[3,2-b]thiophene-based Polymers and Devices. *Adv. Funct. Mater.* **2014**, *24*, 1465−1473.
(12) Hou, J.; Chen, H. Y.; Zhang, S.; Li, G.; Yang, Y. Synthesis, Characterization, and Photovoltaic Properties of a Low Band Gap Polymer Based on Silole-containing Polythiophenes and 2, 1, 3-benzothiadiazole. *J. Am. Chem. Soc.* **2008**, *130*, 16144−16145.
(13) Tamayo, A. B.; Walker, B.; Nguyen, T. Q. A Low Band Gap, Solution Processable Oligothiophene with a Diketopyrrolopyrrole Core for Use in Organic Solar Cells. *J. Phys. Chem. C* **2008**, *112*, 11545−11551.
(14) Liang, Y.; Yu, L. A New Class of Semiconducting Polymers for Bulk Heterojunction Solar Cells with Exceptionally High Performance. *Acc. Chem. Res.* **2010**, *43*, 1227−1236.
(15) Carsten, B.; Szarko, J. M.; Son, H. J.; Wang, W.; Lu, L.; He, F.; Rolczynski, B. S.; Lou, S. J.; Chen, L. X.; Yu, L. Examining the Effect of the Dipole Moment on Charge Separation in Donor-acceptor Polymers for Organic Photovoltaic Applications. *J. Am. Chem. Soc.* **2011**, *133*, 20468−20475.
(16) Dou, L.; Gao, J.; Richard, E.; You, J.; Chen, C. C.; Cha, K. C.; He, Y.; Li, G.; Yang, Y. Systematic Investigation of Benzodithiophene- and Diketopyrrolopyrrole-based Low-bandgap Polymers Designed for Single Junction and Tandem Polymer Solar Cells. *J. Am. Chem. Soc.* **2012**, *134*, 10071−10079.
(17) Zhou, H.; Yang, L.; You, W. Rational Design of High Performance Conjugated Polymers for Organic Solar Cells. *Macromolecules* **2012**, *45*, 607−632.
(18) Hendriks, K. H.; Li, W.; Wienk, M. M.; Janssen, R. A. Small-bandgap Semiconducting Polymers with High Near-infrared Photoresponse. *J. Am. Chem. Soc.* **2014**, *136*, 12130−12136.
(19) Piliego, C.; Frchet, J. M. J. Synthetic Control of Structural Order in N-alkylthieno[3,4-c]pyrrole-4,6-dione-based Polymers for Efficient Solar Cells. *J. Am. Chem. Soc.* **2010**, *132*, 7595−7597.
(20) Zhou, H.; Yang, L.; Stuart, A. C.; Price, S. C.; Liu, S.; You, W. Development of Fluorinated Benzothiadiazole as a Structural Unit for a Polymer Solar Cell of 7% Efficiency. *Angew. Chem., Int. Ed.* **2011**, *50*, 2995−2998.
(21) Guo, S.; Ning, J.; Körstgens, V.; Yao, Y.; Herzig, E. M.; R, S. V.; Müller-Buschbaum, P. The Effect of Fluorination in Manipulating the Nanomorphology in PTB7:$PC_{71}BM$ Bulk Heterojunction Systems. *Adv. Energy Mater.* **2015**, *5*, 1401315.
(22) Hou, J.; Chen, H. Y.; Zhang, S.; Chen, R. I.; Yang, Y.; Wu, Y.; Li, G. Synthesis of a Low Band Gap Polymer and Its Application in Highly Efficient Polymer Solar Cells. *J. Am. Chem. Soc.* **2009**, *131*, 15586−15587.
(23) Alem, S.; Wakim, S.; Lu, J.; Robertson, G.; Ding, J.; Tao, Y. Degradation Mechanism of Benzodithiophene-based Conjugated Polymers When Exposed to Light in Air. *ACS Appl. Mater. Interfaces* **2012**, *4*, 2993−2998.
(24) Razzell-Hollis, J.; Wade, J.; Tsoi, W. C.; Soon, Y.; Durrant, J.; Kim, J. S. Photochemical Stability of High Efficiency PTB7:$PC_{70}BM$ Solar Cell Blends. *J. Mater. Chem. A* **2014**, *2*, 20189−20195.
(25) Lilliedal, M. R.; Medford, A. J.; Madsen, M. V.; Norrman, K.; Krebs, F. C. The Effect of Post-processing Treatments on Inflection Points in Current-voltage Curves of Roll-to-roll Processed Polymer Photovoltaics. *Sol. Energy Mater. Sol. Cells* **2010**, *94*, 2018−2031.
(26) Lin, Z.; Zhang, J. Development of Inverted Organic Solar Cells with TiO_2 Interface Layer by Using Low-temperature Atomic Layer Deposition. *ACS Appl. Mater. Interfaces* **2013**, *5*, 713−718.
(27) Schmidt, H.; Zilberberg, K.; Schmale, S.; Flügge, H.; Riedl, T.; Kowalsky, W. Transient Characteristics of Inverted Polymer Solar Cells Using Titanium Oxide Interlayers. *Appl. Phys. Lett.* **2010**, *96*, 243305.
(28) Kim, G.; Kong, J.; Kim, J.; Kang, H.; Back, H.; Kim, H.; Lee, K. Overcoming the Light-soaking Problem in Inverted Polymer Solar Cells by Introducing a Heavily Doped Titanium Sub-oxide Functional Layer. *Adv. Energy Mater.* **2015**, *5*, 1401298.
(29) Lim, F. J.; Set, Y. T.; Krishnamoorthy, A.; Ouyang, J.; Luther, J.; Ho, G. W. Addressing the Light-soaking Issue in Inverted Organic Solar Cells Using Chemical Bath Deposited Fluorinated Tiox Electron Transport Layer. *J. Mater. Chem. A* **2015**, *3*, 314−322.
(30) Chen, D.; Zhang, C.; Wang, Z.; Zhang, J.; Tang, S.; Wei, W.; Sun, L.; Hao, Y. High Efficient Ito Free Inverted Organic Solar Cells Based on Ultrathin Ca Modified AZO Cathode and Their Light Soaking Issue. *Org. Electron.* **2014**, *15*, 3006−3015.
(31) Pachoumi, O.; Li, C.; Vaynzof, Y.; Banger, K. K.; Sirringhaus, H. Improved Performance and Stability of Inverted Organic Solar Cells with Sol-gel Processed, Amorphous Mixed Metal Oxide Electron Extraction Layers Comprising Alkaline Earth Metals. *Adv. Energy Mater.* **2013**, *3*, 1428−1436.
(32) Reese, M.; Gevorgyan, S.; Jørgensen, M.; Bundgaard, E.; Kurtz, S.; Ginley, D.; Olson, D.; Lloyd, M.; Morvillo, P.; Katz, E. Consensus Stability Testing Protocols for Organic Photovoltaic Materials and Devices. *Sol. Energy Mater. Sol. Cells* **2011**, *95*, 1253−1267.
(33) Manceau, M.; Bundgaard, E.; Carle, J. E.; Hagemann, O.; Helgesen, M.; Sondergaard, R.; Jorgensen, M.; Krebs, F. C. Photochemical Stability of π-conjugated Polymers for Polymer Solar Cells: a Rule of Thumb. *J. Mater. Chem.* **2011**, *21*, 4132−4141.
(34) Wang, W.; Schaffer, C. J.; Song, L.; Körstgens, V.; Pröller, S.; Indari, E. D.; Wang, T.; Abdelsamie, A.; Bernstorff, S.; Müller-Buschbaum, P. In operando Morphology Investigation of Inverted Bulk Heterojunction Organic Solar Cells by GISAXS. *J. Mater. Chem. A* **2015**, *3*, 8324−8331.
(35) Rivaton, A.; Gardette, J. L. Photo-oxidation of Aromatic Polymers. *Angew. Makromol. Chem.* **1998**, *261−262*, 173−188.
(36) Krebs, F. C.; Norrman, K. Analysis of the Failure Mechanism for a Stable Organic Photovoltaic during 10 000 h of Testing. *Prog. Photovoltaics: Res. Appl.* **2007**, *15*, 697−712.
(37) Chambon, S.; Rivaton, A.; Gardette, J. L.; Firon, M. Durability of MDMO-PPV and MDMO-PPV:PCBM Blends Under Illumination in the Absence of Oxygen. *Sol. Energy Mater. Sol. Cells* **2008**, *92*, 785−792.
(38) Hermenau, M.; Riede, M.; Leo, K.; Gevorgyan, S. A.; Krebs, F. C.; Norrman, K. Water and Oxygen Induced Degradation of Small Molecule Organic Solar Cells. *Sol. Energy Mater. Sol. Cells* **2011**, *95*, 1268−1277.
(39) Morlat, S.; Gardette, J. L. Phototransformation of Water-soluble Polymers. I: Photo- and Thermooxidation of Poly(ethylene Oxide) in Solid State. *Polymer* **2001**, *42*, 6071−6079.
(40) Lee, J. Y.; Shin, W. S.; Haw, J. R.; Moon, D. K. Low Band-gap Polymers Based on Quinoxaline Derivatives and Fused Thiophene as Donor Materials for High Efficiency Bulk-heterojunction Photovoltaic Cells. *J. Mater. Chem.* **2009**, *19*, 4938−4945.
(41) Sun, H.; Weickert, J.; Hesse, H. C.; Schmidt-Mende, L. UV Light Protection Through TiO_2 Blocking Layers for Inverted Organic Solar Cells. *Sol. Energy Mater. Sol. Cells* **2011**, *95*, 3450−3454.
(42) Liu, H.; Wu, Z.; Hu, J.; Song, Q.; Wu, B.; Tam, H. L.; Yang, Q.; Choi, W. H.; Zhu, F. Efficient and Ultraviolet Durable Inverted Organic Solar Cells Based on an Aluminum-doped Zinc Oxide Transparent Cathode. *Appl. Phys. Lett.* **2013**, *103*, 043309.

DOI: 10.1021/acsami.5b02383
ACS Appl. Mater. Interfaces 2015, 7, 12119−12127

(43) Street, R.; Davies, D. Kinetics of Light Induced Defect Creation in Organic Solar Cells. *Appl. Phys. Lett.* **2013**, *102*, 043305.
(44) Schaffer, C. J.; Palumbiny, C. M.; Niedermeier, M. A.; Jendrzejewski, C.; Santoro, G.; Roth, S. V.; Müller-Buschbaum, P. A Direct Evidence of Morphological Degradation on a Nanometer Scale in Polymer Solar Cells. *Adv. Mater.* **2013**, *25*, 6760−6764.
(45) Guo, S.; Brandt, C.; Andreev, T.; Metwalli, E.; Wang, W.; Perlich, J.; Müller-Buschbaum, P. First Step into Space: Performance and Morphological Evolution of P3HT:PCBM Bulk Heterojunction Solar Sells Under AM0 Illumination. *ACS Appl. Mater. Interfaces* **2014**, *6*, 17902−17910.
(46) Son, H. J.; Wang, W.; Xu, T.; Liang, Y.; Wu, Y.; Li, G.; Yu, L. Synthesis of Fluorinated Polythienothiophene-co-benzodithiophenes and Effect of Fluorination on the Photovoltaic Properties. *J. Am. Chem. Soc.* **2011**, *133*, 1885−1894.
(47) Verbakel, F.; Meskers, S. C.; Janssen, R. A. Electronic Memory Effects in Diodes from a Zinc Oxide Nanoparticle-polystyrene Hybrid Material. *Appl. Phys. Lett.* **2006**, *89*, 102103.
(48) Trost, S.; Zilberberg, K.; Behrendt, A.; Polywka, A.; Görrn, P.; Reckers, P.; Maibach, J.; Mayer, T.; Riedl, T. Overcoming the "light-soaking" Issue in Inverted Organic Solar Cells by the Use of Al:ZnO Electron Extraction Layers. *Adv. Energy Mater.* **2013**, *3*, 1437−1444.
(49) Massari, J.; Bechara, E. J. H. Generation of Singlet Oxygen by the Glyoxal-peroxynitrite System. *J. Am. Chem. Soc.* **2011**, *133*, 20761−20768.
(50) Kevin, M.; Lee, G. H.; Ho, G. W. Non-planar Geometries of Solution Processable Transparent Conducting Oxide: from Film Characterization to Architectured Electrodes. *Energy Environ. Sci.* **2012**, *5*, 7196−7202.
(51) Ho, P. Y.; Thiyagu, S.; Kao, S. H.; Kao, C. Y.; Lin, C. F. ZnO Nanorod Arrays for Various Low-bandgap Polymers in Inverted Organic Solar Cells. *Nanoscale* **2013**, *6*, 466−471.
(52) Lim, F. J.; Krishnamoorthy, A.; Luther, J.; Ho, G. W. Influence of Novel Fluorosurfactant Modified PEDOT:PSS Hole Transport Layer on the Performance of Inverted Organic Solar Cells. *J. Mater. Chem.* **2012**, *22*, 25057−25064.

DOI: 10.1021/acsami.5b02383
ACS Appl. Mater. Interfaces 2015, 7, 12119−12127